

# Rugged Textile Electrodes for Wearable Devices Obtained by Vapor Coating Off-the-Shelf, Plain-Woven Fabrics

Lushuai Zhang, Marianne Fairbanks, and Trisha L. Andrew\*

Fabrics are pliable, breathable, lightweight, ambient stable, and have unmatched haptic perception. Here, a vapor deposition method is used to transform off-the-shelf plain-woven fabrics, such as linen, silk, and bast fiber fabrics, into metal-free conducting electrodes. These fabric electrodes are resistant to wear, stable after laundering and ironing, and can be body-mounted with little detriment to their performance. A unique by-product of conformally vapor coating plain-woven fabrics is that textile parameters, such as thread material and fabric porosity, significantly affect the conductivity of the resulting fabric electrodes. The resistivities of the electrodes reported herein are linearly, not exponentially, dependent on length, meaning that they can be feasibly incorporated into garments and other large-area body-mounted devices. Further, these fabric electrodes possess the feel, weight, breathability, and pliability of standard fabrics, which are important to enable adoption of wearable devices.

## 1. Introduction

Stretchable, body-mountable, and wearable electronics constitute the frontier of human interface devices that are making possible advanced physiological and performance monitoring,<sup>[1]</sup> new touch/user interfaces,<sup>[2]</sup> and portable power generation,<sup>[3]</sup> to name a few innovations. Many recently reported wearable or body-mountable devices can be classified as fabric/thread approximations. Body-mountable devices are created on strips of thin or ultrathin plastic substrates then plain-woven to resemble a fabric-like sample.<sup>[4]</sup> Alternatively, designer fibers are coated, first, with active layer materials and, second, with a thin protective polymer layer (cladding), and then these cladded fibers are yarned together to approximate threads and yarns found in clothing.<sup>[5]</sup> These fabric/thread imitations yield a variety of notably functional and satisfactorily wearable devices.

Dr. L. Zhang, Prof. T. L. Andrew  
Department of Polymer Science & Engineering  
University of Massachusetts Amherst  
Amherst, MA 01003, USA  
E-mail: tandrew@umass.edu  
Prof. M. Fairbanks  
School of Human Ecology  
Fashion and Design Studies Department  
University of Wisconsin–Madison  
Madison, WI 53706, USA

 The ORCID identification number(s) for the author(s) of this article can be found under <http://dx.doi.org/10.1002/adfm.201700415>.

DOI: 10.1002/adfm.201700415

However, aesthetics and haptic perception can make or break a nascent wearable technology, irrespective of device metrics. There is strong motivation for using something that is already familiar, such as cotton/silk thread, fabrics, and clothes, and imperceptibly adapting it to a new technological application. The pliability, breathability, wearability, and feel of fabrics are unmatched. Especially for skin-mountable devices and smart garments, the intrinsic breathability and feel of fabrics cannot be replicated by devices built on plastic substrates or cladded designer fibers, no matter how thin or flexible these device arrays are.

The approach of starting from a familiar, mass-produced fabric, and coating it with electronically active materials to yield electrodes and supercapacitors has been investigated before.<sup>[6]</sup>

However, the solution processing methods used to coat these fabrics often resulted in either troubling device variations<sup>[7]</sup> or in devices that could not be skin-mountable and laundered.<sup>[8]</sup>

We suggest that solution processed coatings often obfuscate the intrinsic flexibility, breathability, and haptic perception of fabrics. In comparison, vapor deposited coatings are known to be conformal<sup>[9]</sup> and are often thin enough such that the original mechanical properties of the substrate (and not that of the coating) will be the dominant observable.<sup>[10]</sup> Nevertheless, only a few vapor-coated fabric-based electronic components have been demonstrated.<sup>[11]</sup>

Here, we present a small set of robust textile electrodes, made by vapor coating silk/linen/bast fiber fabrics, that can be used as circuit components in smart textiles and other skin-mountable devices. The fabric electrodes we report are unique for the following reasons:

1. Their conductivities are stable to body heat, laundering, ironing, and mechanical deformations.
2. They have the feel, weight, breathability, and pliability of standard fabrics.
3. Their resistivities are linearly, not exponentially, dependent on length, meaning that they can be feasibly incorporated into garments.
4. Their electrical characteristics can be significantly tuned by textile parameters, such as weave density and thread composition, without the need to modify chemistry or processing conditions, thus proving a useful and unexpected control knob with which to create new electronic components for wearable devices.

All these characteristics are a result of the vapor deposition technique used to create our fabric electrodes, and cannot be replicated with solution techniques.

## 2. Results and Discussion

### 2.1. Vapor Coating of Fabric Substrates

Our approach to creating fabric electrodes for wearable devices is to start with common and familiar plain-woven fabrics, such as linen, wool, and silk, and then deposit a thin, metal-free coating onto these fabrics that will transform them into

conductors without altering their characteristic feel, porosity, weight, or mechanical/tensile properties.

Fourteen different off-the-shelf, plain-woven fabrics were coated, including five cotton fabrics with different porosities/weaving densities, three linen fabrics, two silk fabrics, one wool gauze, one bamboo rayon fabric, and two bast fiber fabrics (pineapple fiber fabric and banana fiber fabric). These fabrics were all purchased from a common crafts store and were chosen because of differing thread/fiber composition, surface chemistry, and weave pattern.

Fabrics were coated with a conducting polymer, poly(3,4-ethylenedioxythiophene) (PEDOT) film using a reactive vapor deposition chamber (Figure 1a) whose design was adapted from

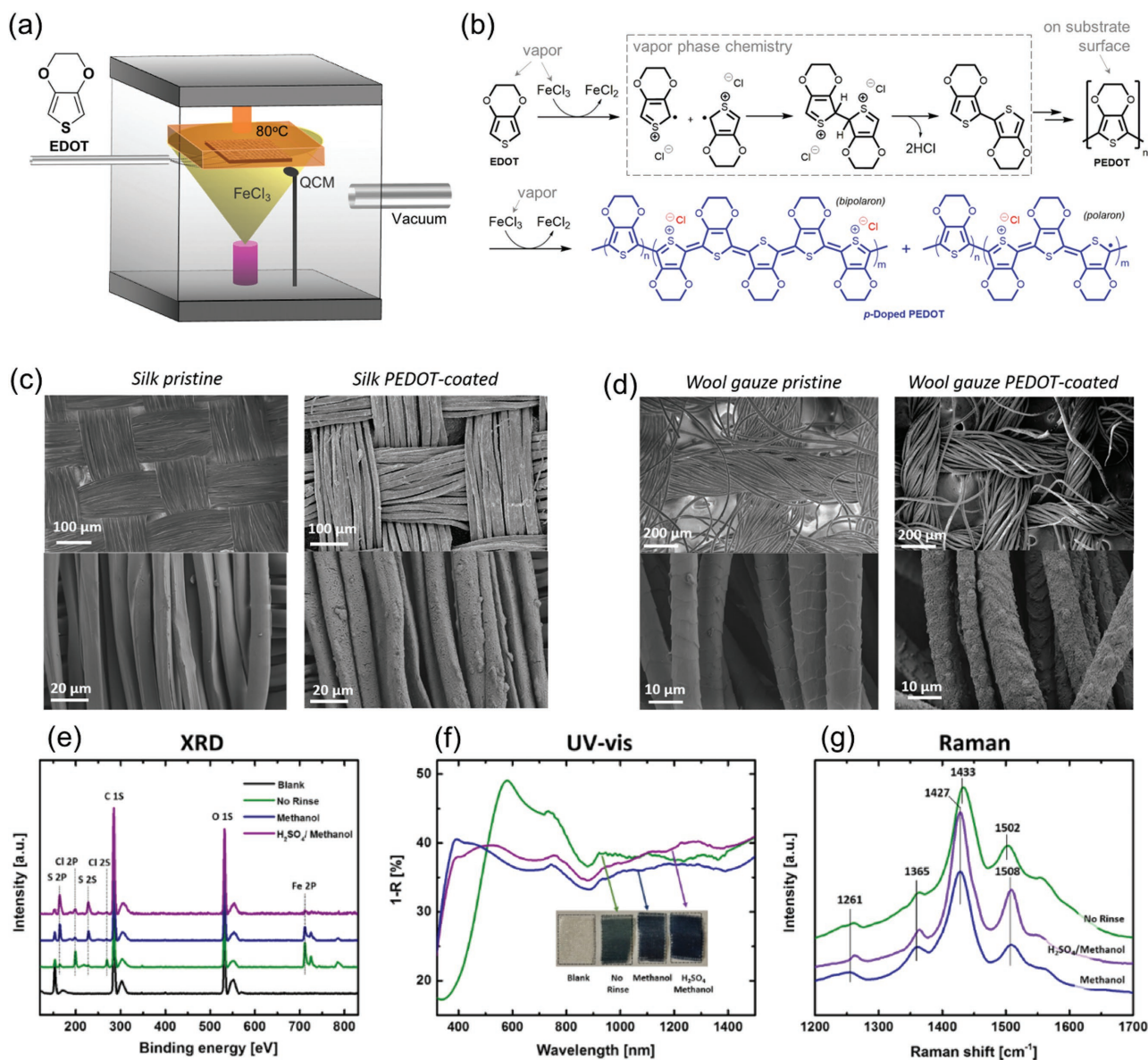


**Figure 1.** a) Illustration of vapor deposition system. b) Chemistry underlying the vapor phase polymerization of EDOT with  $\text{FeCl}_3$  to yield p-doped PEDOT coatings on fabrics. c) SEM images of pristine silk textile and PEDOT-coated silk textile. d) SEM images of pristine wool gauze and PEDOT-coated wool gauze. e) XPS survey scan, f) UV-vis, g) Raman spectra of a 100 nm thick PEDOT film deposited on linen without rinsing (green), rinsed with methanol (blue), or rinsed with 1 M  $\text{H}_2\text{SO}_4$  followed by methanol (purple). A pristine linen textile was also studied by XPS to compare.

previous reports on the in situ vapor phase polymerization of 3,4-ethylenedioxythiophene (EDOT).<sup>[12]</sup> The major components of this chamber include: an electrical furnace to uniformly deliver FeCl<sub>3</sub> vapor to a sample stage situated at 7 in. above the furnace; a 5 × 5 in.<sup>2</sup> heated sample stage; stainless steel tubing with in-line mass flow controller to transport EDOT vapor from outside of the chamber; and an in situ quartz crystal microbalance (QCM) sensor to monitor the EDOT/FeCl<sub>3</sub> flow rates and thickness of the deposited PEDOT film in real time. Additional noble gases can be introduced into the chamber from a second gas inlet to control the process pressure.

Vapor phase oligomerization and polymerization of EDOT is expected to occur in the regions where the EDOT vapor flux intersects with the conical FeCl<sub>3</sub> vapor plume and the resulting EDOT oligomers, which should possess comparatively low kinetic energy, are expected to coat any surface placed within these intersectional regions. A process pressure of 100 mTorr during deposition translates into mean free paths on the order of millimeters for these reactive oligomers.<sup>[13]</sup> Since these mean free paths are commensurate with the surface roughness of woven fabrics, the EDOT oligomers should be able to sample multiple sites before finally adhering to a particular surface, yielding conformal coatings. Additionally, heating the sample stage during deposition should impart lateral mobility along the fabric surface to adsorbed oligomers and, thus, lead to better surface conformality and PEDOT conductivity.<sup>[14]</sup> Stage heating also encourages oligomer–oligomer coupling to form higher molecular weight polymers.<sup>[14]</sup> A postdeposition rinse completely removes residual FeCl<sub>3</sub> trapped in the vapor deposited PEDOT films and yields metal-free, PEDOT-coated fabrics.

The thickness of the growing polymer film inside the chamber is monitored in real time by a QCM sensor situated near the sample stage. The total deposition rate and film thickness values reported by the QCM sensor during vapor deposition arise from both the polymer film and unreacted EDOT/FeCl<sub>3</sub> being deposited onto the sensor surface. Thickest polymer films are obtained after rinsing when the EDOT and FeCl<sub>3</sub> flow rates are matched during deposition. Unreacted EDOT or FeCl<sub>3</sub> remain trapped in the films if their flow rates are mismatched, which are leached out of the film during rinsing, leading to significantly lower coating thicknesses than measured by the QCM sensor during deposition. A corrective tooling factor to account for this discrepancy was obtained as described in the Experimental Section. Taking this correction into account, typical polymer growth rates are 10–15 nm min<sup>-1</sup> for a substrate stage temperature of 80 °C.

Figure 1c,d shows scanning electron microscopy (SEM) images of a silk fabric and wool gauze before and after PEDOT coating (and rinsing). The coating thickness is ≈200 nm and the two fabrics are observed to turn royal blue after PEDOT deposition. Large-area SEM images of the pristine fabrics reveal the interwoven structure of several threads, each of which are comprised of fibril bundles as shown in small area images. Highly uniform and conformal coatings are formed on all fabric surfaces that are exposed to the reactive vapor in the chamber, without any special pretreatment or fixing steps. Further, the PEDOT film is uniformly deposited (macroscopically) over the entire 1 sq. in. surface of the fabric while also conformally wrapping (microscopically) the curved surface of each exposed fibril

of the threads constituting the fabric. The high conformality of the surface coating is particularly apparent in the SEM image of PEDOT-coated wool gauze, where the PEDOT film contours to all the exposed surface features of the fabric with high fidelity over multiple length scales. Cross-section SEM images shown in Figure S1 (Supporting Information) confirm that the PEDOT film is purely a surface coating and that the bulk of fibrils/threads are not swelled or dyed by the polymer.

All the aforementioned 14 fabrics were successfully vapor coated with PEDOT without any pretreatment steps, irrespective of surface chemistry, thread/yarn composition, and weave density. The PEDOT coating did not change the feel of any of the fabrics, as determined by touching the fabrics with bare hands before and after coating. Further, the coating did not increase the weight of the fabrics by more than 2%.

## 2.2. Chemical Characterization of PEDOT Films on Fabrics

Chemical characterization of a 100 nm thick PEDOT coating on a linen fabric is displayed in Figure 1e–g. Figure 1e shows the X-ray photoelectron spectroscopy (XPS) survey scan of a pristine linen fabric (black), and the same fabric immediately after PEDOT coating (green), after rinsing with methanol (blue), and after rinsing with 1 M sulfuric acid followed by methanol (H<sub>2</sub>SO<sub>4</sub>/MeOH, purple). All spectra were normalized to the C 1S peak. The Fe 2P peak indicates the existence of residual FeCl<sub>3</sub> in the as-deposited film, which is partially removed by a methanol rinse and completely removed after a 1 M H<sub>2</sub>SO<sub>4</sub>/MeOH rinse, as confirmed the absence of a Fe 2P peak in this sample. The residual Cl 2S and Cl 2P peaks in the rinsed samples are ascribed to the Cl<sup>-</sup> counterions in p-doped PEDOT.

Figure 1f shows the 1-Reflectance spectra (recorded with an integrating sphere) of vapor deposited PEDOT films on linen textiles. The inset optical images include a pristine linen textile, and a linen textile coated with PEDOT before rinsing, after rinsing with methanol and after rinsing with 1 M H<sub>2</sub>SO<sub>4</sub>/MeOH. All 1-Reflectance spectra show similarly strong absorption bands above 800 nm, which is typically assigned to the bipolaron absorption manifold of p-doped PEDOT.<sup>[15]</sup> This characteristic bipolaron absorption feature agrees with the XPS results revealing the persistence of chloride ions in the rinsed films, which would be present as counterions for the p-doped form of PEDOT.

Postdeposition rinsing causes a decreased absorption between 500 and 800 nm (likely due to slight dedoping accompanying the loss of FeCl<sub>3</sub>), accompanied by a correlated increase between 400 and 500 nm, arising from the backbone  $\pi \rightarrow \pi^*$  transition of undoped PEDOT.<sup>[16]</sup> The spectra of the MeOH and H<sub>2</sub>SO<sub>4</sub>/MeOH rinsed samples resemble each other, implying that 1 M H<sub>2</sub>SO<sub>4</sub> does not affect the doping level of the PEDOT films. The degree of dedoping upon rinsing is found to vary for different fabrics, with nylon, silk, and banana/pineapple fabrics demonstrating little to no dedoping with rinsing (as determined by the lack of a PEDOT<sup>0</sup> absorbance band at 400 nm after rinsing, see Figure S2 in the Supporting Information).

The Raman spectra in Figure 1g also support the partially changed doping level of the PEDOT films on linen fabrics after

rinsing. The peaks at 1261 and 1365  $\text{cm}^{-1}$  are attributed to the  $C_{\alpha}=C_{\alpha'}$  inter-ring stretching and  $C_{\beta}-C_{\beta}$  stretching,<sup>[17]</sup> respectively, and do not shift upon rinsing. The peak at 1427  $\text{cm}^{-1}$  in the sample after rinsing corresponds to the  $C_{\alpha}=C_{\beta}$  stretching of undoped PEDOT<sup>0</sup>.<sup>[17]</sup> Before rinsing, the  $C_{\alpha}=C_{\beta}$  stretching peak is right-shifted and broadened, corresponding to p-doped, PEDOT<sup>+</sup>. The presence of PEDOT<sup>0</sup> after rinsing is also supported by the right-shifted peak at 1508  $\text{cm}^{-1}$  compared to the peak at 1502  $\text{cm}^{-1}$  of PEDOT<sup>+</sup>.

In sum, the XPS, UV-vis and Raman spectra confirm that p-doped PEDOT films are formed on fabric surfaces and remain chemically intact after rinsing. Residual  $\text{FeCl}_3$  from the vapor deposition process is shown to be completely removed by a  $\text{H}_2\text{SO}_4$ /methanol rinse.

### 2.3. Chemical and Mechanical Stability of Vapor Deposited PEDOT Coatings on Fabrics

The chemical and mechanical stabilities of our vapor deposited PEDOT coatings were quantified by monitoring the absorption (1-Reflectance) spectrum of a PEDOT-coated silk textile (100 nm thick coating) at three different wavelengths after various stress tests. Harsh conditions were applied on the same sample in series, including rubbing with bare hands, scraping with the sharp end of a metal spatula, heating on a hot plate at 50 °C for 10 min, laundering (vigorously stirring with commercial laundry detergent for 10 min, followed by clean water rinsing), wrinkling/crumpling followed by ironing with a household clothes iron. After all these conditions, the edge of textile is to some degree worn, yet the polymer coating remains intact. **Figure 2a** displays the (1-Reflectance) spectrum of a freshly PEDOT-coated silk fabric and the three wavelengths (400, 700, and 1000 nm) at which the coating stability was monitored. **Figure 2b** shows that the absorption values of the PEDOT coating on silk do not change after being subjected to various deformation and friction events, indicating that the PEDOT coating is resilient to common wear and tear that would be experienced by garments and other wearable devices. Further, based on the minimal change in the absorption band at 1000 nm (arising from the PEDOT bipolaron), we conclude that neither laundry detergent nor mechanical stresses affect the doping level of the PEDOT coating. Videos of this PEDOT-coated silk fabric being subjected to various stress tests are provided as in the Supporting Information.

### 2.4. Conductivity of PEDOT-Coated Fabrics

The large-area resistances of various PEDOT-coated fabric squares were measured using an Ohmmeter by connecting alligator clips to two edges of the fabric samples. **Figure 3a** displays such a resistivity measurement for a  $4 \times 4 \text{ in.}^2$  pineapple fiber fabric coated with a 500 nm thick PEDOT film. Alligator clips were connected to the fabric square in the horizontal, vertical, or diagonal directions. As seen in the pictures, the PEDOT-coated fabric acts as a classic 2D conductor, with the measured resistance displaying distance dependence but direction independence. The sheet resistance of this fabric is 200  $\Omega$  per

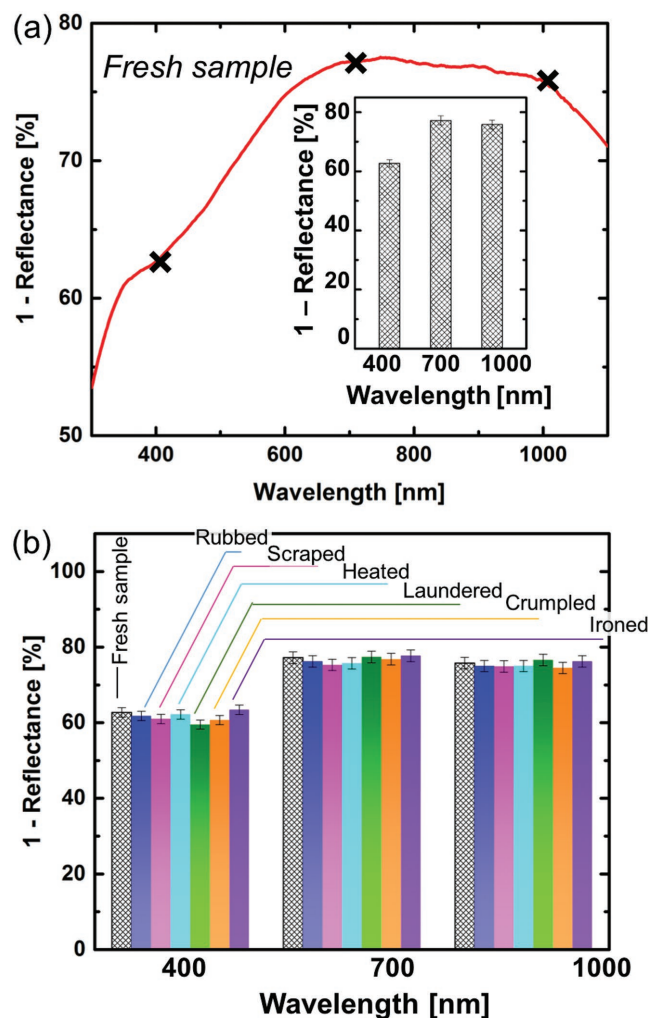


**Figure 2.** a) 1-Reflectance spectrum of a 100 nm thick PEDOT coating on a silk fabric. The inset shows the three data points extracted from the spectrum, corresponding to 400, 700, and 1000 nm. b) 1-Reflectance values measured for the same sample after rubbing with bare hands, scraping, heating, laundering, crumpling, and ironing.

square, which is comparable to that of commercial indium tin oxide (ITO) on glass (150  $\Omega$  per square). **Figure 3b** reveals that sample deformation does not affect fabric resistance: the measured resistance remains unchanged between a flat sample and a 180° curved sample, and between a folded or unfolded sample (see Movie S1 of folding the textile in the Supporting Information). Such insensitivity to physical stress and movement is integral for functional components of wearable electronics.

We also varied the contact area to confirm that the resistance values obtained during these large-area measurements cannot be ascribed to contact resistance between the fabric and an Ohmmeter probe. Large-area resistance values matching those displayed in **Figure 3a** were obtained if either the number of threads physically contacted to an alligator clip was varied or if the tapered probe tip from a micromanipulator was used to contact the fabric to an Ohmmeter.

Notably, the resistance of the PEDOT-coated fabrics increases linearly, not exponentially, with measurement distance

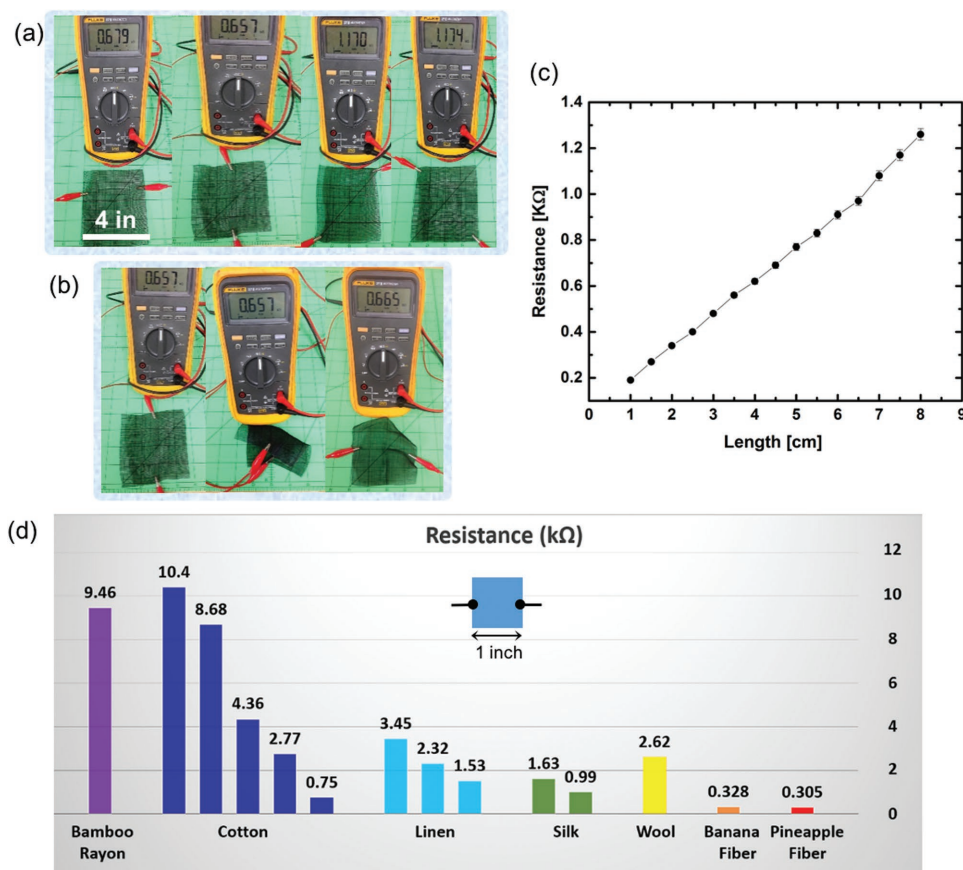


**Figure 3.** a) Large-area resistance measurements of a  $4 \times 4$  in.<sup>2</sup> pineapple fiber fabric coated with a 500 nm thick PEDOT film. b) Large-area resistance measurements when the same  $4 \times 4$  in. fabric is folded or crumpled. c) Resistivity versus length measured along the edge for a  $4 \times 4$  in. square of pineapple fiber fabric coated with 200 nm PEDOT. d) Summary of resistances measured for  $1 \times 1$  in. squares of different fabrics vapor coated with 100 nm PEDOT. Each bar within a fabric family represents a different commercially available fabric (see Table S1 in the Supporting Information for fabric codes).

(Figure 3c). This behavior is similar to that of the copper or silver-coated cloths used for electromagnetic shielding.<sup>[18]</sup> Other conductive materials that have been previously used to create fiber electrodes, such as carbon nanomaterials, typically display exponential increases in resistance with increasing conduction length.<sup>[19]</sup>

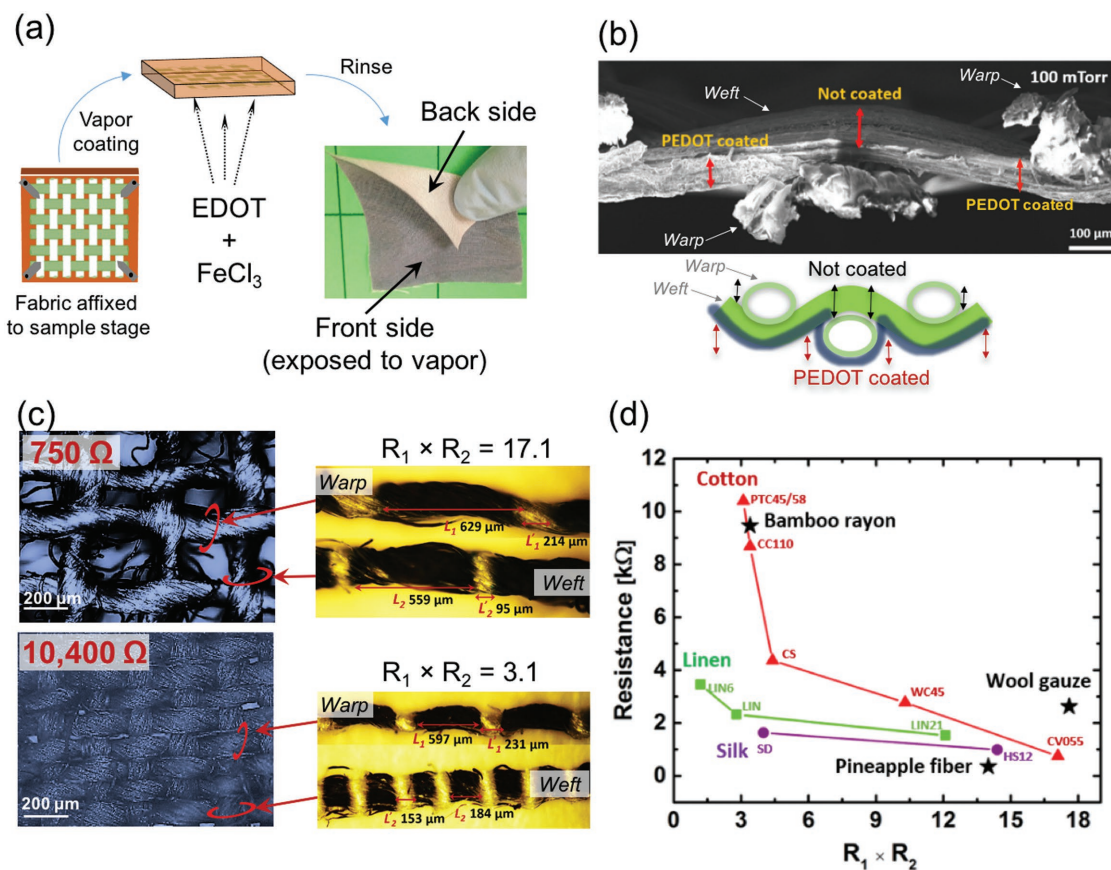
### 2.5. Textile Parameter Effects on Conductivity

Figure 3d plots the large-area resistance values measured for 14 different plain-woven fabrics coated with PEDOT (100 nm), grouped by thread material. For simplicity, the fabric codes for each of the coated samples are omitted from the figure but are listed in Table S1 (Supporting Information). PEDOT films were deposited on  $1 \times 1$  in.<sup>2</sup> squares of all 14 fabrics simultaneously in the same deposition run. The optical images and SEM images of all PEDOT-coated textiles are shown in Figure S3 (Supporting Information). A large variation in the resistances of the 14 different samples is observed. Further, two different trends are evident: the large-area resistance of each fabric square is, first, affected by its constituent threads/fibers (linen vs silk vs wool, etc.) and,

second, by the porosity of the fabric square, as determined by its weave density.

Thread/fiber effects were studied first. Single threads were pulled out from each of the 14 different woven fabrics and, then, vapor coated with 100 nm thick PEDOT. Each thread was 3 in. long and was observed to be wrapped in a uniform PEDOT surface coating after vapor deposition/rinsing. Figure S4 (Supporting Information) summarizes the resistivities of the various PEDOT-coated threads thus obtained. To synopsise, the trend in the resistances observed for different types of PEDOT-coated threads is exactly the same as that observed for PEDOT-coated fabrics. Therefore, the electrical resistivity of a PEDOT-coated plain-woven fabric can, to first degree, be predicted by the identity of its constituent threads.

Families of PEDOT-coated, plain-woven cotton, linen, and silk fabrics exhibit a clear trend where the more porous textiles lead to lower large-area resistances. This trend applies to all samples of different materials: the tight-woven bamboo rayon has a resistance of 9.46 k $\Omega$ , among the highest observed values, while the porous wool gauze has a resistance of 2.62 k $\Omega$ , among the lowest values. The lowest large-area resistance can be obtained on PEDOT-coated pineapple fiber or banana fiber textile, with each giving rise to a resistance of  $\approx 300 \Omega$ .



**Figure 4.** a) Cartoon of a pristine fabric affixed to the sample stage for vapor coating and an optical image of PEDOT-coated silk fabric. b) SEM image of a cross-section of a PEDOT-coated banana fiber fabric, showing that only one face is coated with PEDOT. The PEDOT coating is 1 μm thick. c) Optical images of PEDOT-coated cotton textiles CV055 (top) and PTC45/58 (bottom), and threads pulled from these fabrics after PEDOT coating. The black regions are PEDOT coated, and the yellow regions are uncoated. The length of the regions were measured by the software Advanced Spot.  $R_1$  and  $R_2$  refer to the PEDOT-coated/uncoated length ratios for the warp and weft threads, respectively. d) Plot of resistances of 1 × 1 in.<sup>2</sup> size textiles versus  $R_1 \times R_2$ .

To gain a quantitative understanding of the apparent effect of fabric porosity on conductivity, the macro- and microscopic properties of the vapor deposited PEDOT coatings on various fabrics need to be considered. **Figure 4a** shows a cartoon illustration of the sample stage of our vapor deposition chamber with an affixed fabric. During deposition, only one face of the fabric is exposed to the EDOT/FeCl<sub>3</sub> reactive vapor and is, therefore, coated with PEDOT, while the other face remains contacted to the sample stage and, therefore, uncoated. This is best illustrated by the optical image of a tight woven silk fabric after PEDOT deposition and rinsing (**Figure 4a**), where the dark blue color arises from the PEDOT coating and the light color belongs to the pristine silk. In the same vein, **Figure 4b** shows a cross-section SEM image of a PEDOT coated and rinsed banana fiber fabric, specifically focusing on a weave intersection of two threads. For each thread, regions that are exposed to the reactive vapors are coated with polymer (bright), whereas regions that are buried behind other threads due to the weave pattern have no polymer coating (dark).

Effectively, the “warp” and “weft” threads of each plain-woven fabric act as each other’s shadow mask, creating a broken but periodic linear pattern of PEDOT coatings on each thread. This

broken linear pattern is depicted in **Figure 4c**, which shows optical images of individual warp and weft threads pulled out of two different plain-woven fabrics after vapor coating. The dark black sections contain a PEDOT coating, while the bright yellow sections are regions that were buried at weave intersections and, therefore, remained uncoated. The representative length of each region is shown in the images. Due to the presence of uncoated regions along each thread when a prewoven fabric is vapor coated, a single thread cannot act as a continuous wire. Instead, a charge carrier has to be scattered at an orthogonal thread at each weave intersection (**Figure S5**, Supporting Information), which results in an increased effective conduction length.

To quantify this phenomenon, we use a parameter,  $R$ , defined as the ratio of the length of PEDOT-coated sections ( $L_n$ ) to the length of uncoated sections ( $L'_n$ ) on each thread (**Figure 4c** and **Figure S6** (Supporting Information)).  $R_1$  and  $R_2$  denote the coated-to-uncoated ratio of the warp and weft threads, respectively.  $R_n$  values can be understood as quantifying the probability for a charge to continuously travel in 1D along a single thread without being scattered at intersections. The product of  $R_1$  and  $R_2$  can be considered as the 2D

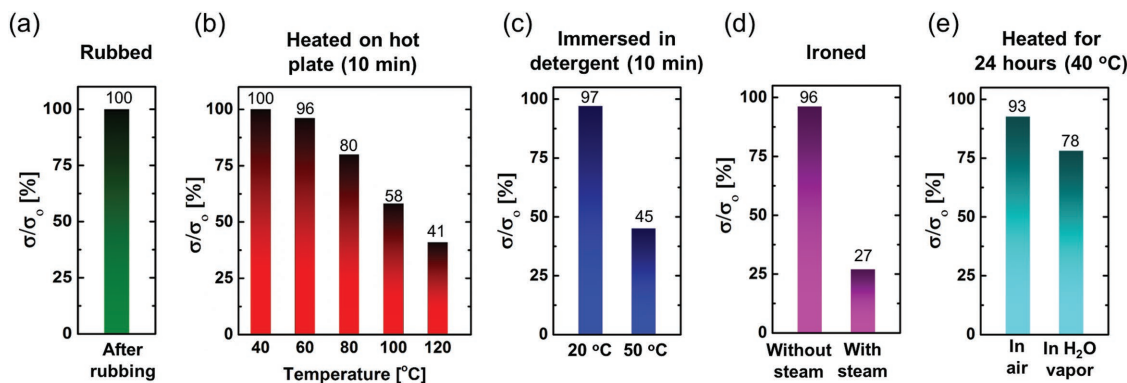


**Figure 5.** Effects of a) rubbing/scraping, b) heating, c) laundering, d) ironing, and e) extended heating on the conductivity of a PEDOT-coated pineapple fiber fabric.

analog of the same probability. The optical images of warp/weft threads pulled from all 14 PEDOT-coated textiles are shown in Figure S7 (Supporting Information) and all pertinent  $R$  values are listed in Table S2 (Supporting Information). As summarized in Figure 4d, fabric electrodes with larger  $R_1 \times R_2$  values, which correspond to porous or open-weave fabrics, consistently have lower resistances within each fabric family.

The effects of fabric porosity on large-area resistance are significant. Figure 4c shows optical images of two PEDOT-coated cotton fabrics, a porous CV055 (top) and a tight-woven PTC45/58 (bottom), simultaneously coated with a 100 nm thick PEDOT film. The porous fabric displays a resistance of 750  $\Omega$ , whereas the tight-woven fabric has a resistance of 10 400  $\Omega$ , despite being comprised of the same thread material.

In summary, the electrical resistivity of a PEDOT-coated plain-woven fabric electrode can be tuned, first, by choosing its constituent threads and, second, by adjusting its porosity (weave density).

## 2.6. Stability of Fabric Conductivity

The electrical stability of the PEDOT-coated fabric electrodes were investigated using a representative PEDOT-coated (100 nm) pineapple fiber fabric ( $2 \times 1$  in.<sup>2</sup> swatch). Conductivities were measured using a four-point probe after various stress tests and the values plotted as the ratio of the remaining conductivity to the initial conductivity ( $\sigma/\sigma_0$ ). The conductivity of this fabric is 298 S cm<sup>-1</sup>, which is similar to that reported for commercial, conductive-grade PEDOT:PSS. This conductivity value remained constant even after storing the PEDOT-coated fabric on a benchtop, under air, for six months.

Figure 5a shows the remaining conductivity after the fabric was heated on a hot plate for 10 min under air, at temperatures ranging from 40 to 120 °C. The fabric electrodes reported herein demonstrate stable conductance upto 60 °C and can, therefore, be expected to maintain their performance when body-mounted (the core body temperature at rest is 37 °C).

Fabric conductivity remains unchanged after being washed with laundry detergent in room temperature water, though the conductivity decreases if the fabric is washed in hot water. Fabric conductivity also remains unchanged after ironing with

a commercial household iron in either the “Wool” or “Silk” mode, though a decrease in conductivity is observed after steam ironing.

The common observation here is that hot water is detrimental the conductivity of the PEDOT-coated fabric electrode. Therefore, we investigated whether atmospheric humidity would affect the electrical performance of these electrodes by heating two different PEDOT-coated (100 nm) pineapple fiber fabrics on a hot plate at 40 °C for 24 h. One sample was heated in air. The other was heated in humid environment, simulated by placing both the fabric sample and a shallow jar of water on the hot plate and covering both with an inverted crystallization dish. Slight loss in conductivity is observed after the fabric electrode is exposed to a humid atmosphere.

To summarize, the electrical properties of the fabric electrodes reported herein are stable to body heat, cold laundering, and dry ironing.

## 3. Conclusion

Having varied approaches to making a wearable device is integral to grow this nascent technology to maturity. Textile scientists have traditionally shied away from using vapor deposition methods to create various textile-based electronics because of the perceived difficulty and high cost of scaling up vapor coating techniques to satisfy the high volume demand of the textile industry.<sup>[7]</sup> However, advancements made over the past decade have resulted in the use of vapor deposition methods to stain-guard carpets, lubricate large-area mechanical components,<sup>[20]</sup> and protect microelectronic devices,<sup>[9]</sup> demonstrating that vapor coating methods are indeed conducive to large-scale manufacturability.

Here, we used a vapor coating method to transform familiar, off-the-shelf, plain-woven fabrics, such as linen, silk, and bast fiber fabrics, into metal-free conducting electrodes. These conductive coatings are resistant to wear, stable after laundering and ironing, and can be body-mounted with little detriment to their performance. A unique by-product of conformally vapor coating plain-woven fabrics is that textile parameters, such as thread material and fabric porosity, significantly affect the conductivity of the resulting fabric electrodes.

The electrical properties of these fabric electrodes are stable to bending/folding, body heat, cold laundering, and dry ironing. These properties are rare among coated electronic fabrics. Additionally, their resistivities are linearly, not exponentially, dependent on length, meaning that our fabric electrodes can be feasibly incorporated into garments and other large-area body-mounted devices. Further, these fabric electrodes possess the feel, weight, breathability, and pliability of standard fabrics, which are important to enable adoption of wearable devices.

#### 4. Experimental Section

**General Considerations:** All chemicals were purchased from Sigma-Aldrich and used without further purification. XPS was carried out with a Physical Electronics Inc. 5000 Series spectrophotometer. SEM was performed using a FESEM Magellan 400. Conductivities were calculated from resistivity measurements made using a home-built four-point probe test station. Film thicknesses were measured on a Veeco Dektak 150 profilometer.

**Vapor Coating of Fabrics:** Vapor phase polymerization of EDOT was carried out in a custom-built cube-shaped stainless steel chamber adapted from previous reports. The pressure inside the chamber was tuned between 100 and 500 mTorr (Figure S8, Supporting Information) by introducing and controlling an argon gas flow, in addition to the monomer and oxidant flux. A solid oxidant, typically  $\text{FeCl}_3$ , was sublimed inside the chamber using a Luxel crucible heater. A glass ampule containing EDOT was heated with resistive heating tape to 80 °C and the monomer vapor was introduced into the evacuated chamber via a side inlet, controlled by a needle valve. The temperature of the substrate stage inside the chamber was varied between 30 and 80 °C for various textiles. After vapor deposition, the coated substrates were rinsed with 1 M aqueous  $\text{H}_2\text{SO}_4$  followed by copious amounts of methanol under air to remove residual monomer and oxidant from the polymer films.

A corrective tooling factor for the readout obtained from the QCM sensor was obtained as follows. Silicon substrates were coated with films of varying thickness ("QCM reported") at three different monomer:oxidant flow rate ratios, rinsed with  $\text{H}_2\text{SO}_4$ /methanol, and the resulting film thickness ("actual thickness") measured using a profilometer. A tooling factor was obtained by taking the ratio of the actual film thickness after rinsing to the thickness reported by the QCM sensor during deposition. The tooling factor was found to be 0.5 for all monomer:oxidant flow rate ratios.

As an added quantification tool, a  $1 \times 1 \text{ cm}^2$  silicon square "test coupon" was affixed to the sample stage next to the desired fabric samples for each fabric coating run, and the thickness of the PEDOT coating on this test coupon was measured using a profilometer after rinsing. The measured coating thickness on this test coupon was assumed to match the thickness of the conformal PEDOT coating on fabrics.

#### Supporting Information

Supporting Information is available from the Wiley Online Library or from the author.

#### Acknowledgements

The authors gratefully acknowledge financial support from the US Air Force Office of Scientific Research, under Agreement No.

FA9550-14-1-0128. T.L.A. also gratefully acknowledges partial support by the David and Lucille Packard Foundation.

#### Conflict of Interest

The authors declare no conflict of interest.

#### Keywords

conducting polymers, electrodes, vapor coatings, wearable electronics

Received: January 22, 2017

Revised: March 6, 2017

Published online:

- [1] D.-H. Kim, N. Lu, R. Ma, Y.-S. Kim, R.-H. Kim, S. Wang, J. Wu, S. M. Won, H. Tao, A. Islam, K. J. Yu, T.-I. Kim, R. Chowdhury, M. Ying, L. Xu, M. Li, H.-J. Chung, H. Keum, M. McCormick, P. Liu, Y.-W. Zhang, F. G. Omenetto, Y. Huang, T. Coleman, J. A. Rogers, *Science* **2011**, 333, 838.
- [2] G. Schwartz, B. C.-K. Tee, J. Mei, A. L. Appleton, D. H. Kim, H. Wang, Z. Bao, *Nat. Commun.* **2013**, 4, 1859.
- [3] T. F. O'Connor, A. V. Zaretski, S. Savagatrup, A. D. Printz, C. D. Wilkes, M. I. Diaz, E. J. Swayer, D. J. Lipomi, *Sol. Energy Mater. Sol. Cells* **2016**, 144, 438.
- [4] a) M. Kaltenbrunner, M. S. White, E. D. Glowacki, T. Sekitani, T. Someya, N. S. Sariciftci, S. Bauer, *Nat. Commun.* **2012**, 3, 770; b) M. Kaltenbrunner, T. Sekitani, J. Reeder, T. Yokota, K. Kuribara, T. Tokuhara, M. Drack, R. Schwodiauer, I. Graz, S. Bauer-Gogonea, S. Bauer, T. Someya, *Nature* **2013**, 499, 458; c) M. S. White, M. Kaltenbrunner, E. D. Glowacki, K. Gutnichenko, G. Kettlgruber, I. Graz, S. Aazou, C. Ulbricht, D. A. M. Egbe, M. C. Miron, Z. Major, M. Scharber, T. Sekitani, T. Someya, S. Bauer, N. S. Sariciftci, *Nat. Photonics* **2013**, 7, 811; d) M. Hamedi, R. Forchheimer, O. Inganas, *Nat. Mater.* **2007**, 6, 357.
- [5] a) Z. B. Yang, J. Deng, X. L. Chen, J. Ren, H. S. Peng, *Angew. Chem. Int. Ed.* **2013**, 52, 13453; b) M. R. Lee, R. D. Eckert, K. Forberich, G. Dennler, C. J. Brabec, R. A. Gaudiana, *Science* **2009**, 324, 232; c) Z. B. Cai, L. Li, J. Ren, L. B. Qiu, H. J. Lin, H. S. Peng, *J. Mater. Chem. A* **2013**, 1, 258; d) L. X. Zheng, X. F. Zhang, Q. W. Li, S. B. Chikkannanavar, Y. Li, Y. H. Zhao, X. Z. Liao, Q. X. Jia, S. K. Doorn, D. E. Peterson, Y. T. Zhu, *Adv. Mater.* **2007**, 19, 2567; e) Z. B. Yang, J. Deng, X. L. Chen, J. Ren, H. S. Peng, *Angew. Chem. Int. Ed.* **2013**, 52, 13453; f) R. Ma, J. Lee, D. Choi, H. Moon, S. Baik, *Nano Lett.* **2014**, 14, 1944; g) J. A. Lee, M. K. Shin, S. H. Kim, H. U. Cho, G. M. Spinks, G. G. Wallace, M. D. Lima, X. Lepro, M. E. Kozlov, R. H. Baughman, S. J. Kim, *Nat. Commun.* **2013**, 4, 1970.
- [6] a) K. Jost, C. R. Perez, J. K. McDonough, V. Presser, M. Heon, G. Dion, Y. Gogotsi, *Energy Environ. Sci.* **2011**, 4, 5060; b) L. B. Hu, M. Pasta, F. L. Mantia, L. F. Cui, S. Jeong, H. D. Deshazer, J. W. Choi, S. M. Han, Y. Cui, *Nano Lett.* **2010**, 10, 708; c) C. Das, B. Jain, K. Krishnamoorthy, *Chem. Commun.* **2015**, 51, 11662; d) Y. Guo, M. T. Otley, M. Li, X. Zhang, S. K. Sinha, G. M. Treich, G. A. Sotzing, *ACS Appl. Mater. Interfaces* **2016**, 8, 26998; e) T. Bashir, M. Skrifvars, N. K. Persson, *Polym. Adv. Technol.* **2015**, 22, 2214.
- [7] K. Jost, G. Dion, Y. Gogotsi, *J. Mater. Chem. A* **2014**, 2, 10776.
- [8] M. Stoppa, A. Chiolerio, *Sensors* **2014**, 14, 11957.

- [9] K. M. Vaeth, K. F. Jensen, *Adv. Mater.* **1999**, *11*, 814.
- [10] K. K. S. Lau, K. K. Gleason, *Macromolecules* **2006**, *39*, 3688.
- [11] D. Bhattacharyya, R. M. Howden, D. C. Borrelli, K. K. Gleason, *J. Polym. Sci. B* **2012**, *50*, 1329.
- [12] W. E. Tenhaeff, K. K. Gleason, *Adv. Funct. Mater.* **2008**, *18*, 979.
- [13] D. C. Borrelli, S. Lee, K. K. Gleason, *J. Mater. Chem. C* **2014**, *2*, 7223.
- [14] S. G. Im, K. K. Gleason, *Macromolecules* **2007**, *40*, 6552.
- [15] H. Goktas, X. Wang, N. D. Boscher, S. Torosian, K. K. Gleason, *J. Mater. Chem. C* **2016**, *4*, 3403.
- [16] H. Meier, U. Stalmach, H. Kolshorn, *Acta Polym.* **1997**, *48*, 379.
- [17] a) R. M. Howden, E. D. McVay, K. K. Gleason, *J. Mater. Chem. A* **2013**, *1*, 1334; b) M. Stavytska-Barba, A. M. Kelley, *J. Phys. Chem. C* **2010**, *114*, 6822.
- [18] Shielding & Conductive Fabrics, <http://www.lessemf.com/fabric.html> (accessed: January 2017).
- [19] a) J. T. Masden, N. Giordano, *Phys. Rev. Lett.* **1982**, *49*, 819; b) P. J. de Pablo, C. Gomez-Navarro, J. Colchero, P. A. Serena, J. Gomez-Herrero, A. M. Baro, *Phys. Rev. Lett.* **2002**, *88*, 036804; c) L. K. Randeniya, A. Bendavid, P. J. Martin, C. D. Tran, *Small* **2010**, *6*, 1806.
- [20] P. Kovacic, G. del Hierro, W. Livernois, K. K. Gleason, *Mater. Horiz.* **2015**, *2*, 221.